

Signals in non-irradiated and irradiated single sided silicon detectors

G. Kramberger ¹, V. Cindro, M. Mikuz

Institute Jožef Stefan and Department of Physics, University of Ljubljana, SI-1000 Ljubljana, Slovenia

Abstract

A simulation of signals in silicon microstrip detectors ($p^+ - n - n^+$) has been written. Electron-hole pairs are created by electrons from ^{90}Sr beta source with Landau fluctuations considered. Simulated induced currents calculated according to Ramo's theorem are integrated and shaped. For irradiated sensors, trapping is included in the drift simulation. Using many Monte Carlo generated events, detector's charge collection efficiency is calculated as a function of shaping time, applied voltage, and temperature. Results are compared with CCE measurements of unirradiated and irradiated strip detectors using 25ns shaping (SCT 32A) readout chip.

PACS: 61.80.-x; 29.40.Wk

Key words: Full depletion voltage; Electric field, LHC detectors

1 Introduction

Future experiments at LHC will extensively use silicon microstrip detectors for tracking of charged particles. High luminosity and large proton-proton inelastic cross section will result in high fluences of heavy particles to which microstrip detectors will be exposed. So for example the Atlas Semiconductor Tracker will be exposed to fluences up to $1.5 \times 10^{14} \text{ cm}^{-2}$ 1 MeV neutron non-ionizing energy loss (NIEL) equivalent. The dislocation of atoms and related radiation damage will be caused mainly by neutrons and pions [1]. Radiation

¹ Corresponding author; Address: Jožef Stefan Institute, Jamova 39, SI-1000 Ljubljana, Slovenia. Tel: (+386) 1 4773512, fax: (+386) 1 4257074, e-mail: Gregor.Kramberger@ijs.si

damage will cause the change of full depletion voltage (FDV), increase of leakage current and trapping of the drifting charge. These effects have been studied after irradiation of diodes, for example in [2–4] as well as after irradiation of microstrip detectors [5,6]. High FDV results in a danger of electrical breakdown and together with increased leakage current puts additional demands on cooling systems which are difficult to be fulfilled since mass in the trackers has to be kept as low as possible. Short bunch crossing time (BCT= 25 ns) and large number of created particles require short shaping times of readout electronics in order to relate signals with corresponding bunch crossings. A part of charge generated in the detector by an ionizing particle is lost due to trapping since detrapping times are much longer than the electronic shaping times. The drift time and thus also trapping probability during drift can be decreased if detectors are operated at voltages well exceeding FDV.

It is important to determine the bias voltage necessary for efficient operation of detectors already in the design phase of experiments. Many measurements of signal dependence versus bias voltage exist. We have performed a simulation of silicon microstrip detectors together with readout electronics in order to get a better insight into the parameters important for efficient detector operation. To complement previous simulations [8,9] the emphasis was given to the study of bias voltage dependence of signal before and after irradiation of detectors. The drift-induced current was shaped with different shaping circuits. Results were compared with measurements for non-irradiated detectors as well as for detectors irradiated with neutrons to two different fluences ($\Phi_{eq} = 0.5 \times 10^{14} \text{ cm}^{-2}$ and $1.5 \times 10^{14} \text{ cm}^{-2}$).

2 Simulation

2.1 Induced current

Electrons from a collimated ^{90}Sr source ($\cos\theta > 0.99$) were tracked through the detector using the GEANT package. Only electrons that penetrate through the detector and a 0.1 mm Al plate (thin foil window in the detector protection box) were considered in the simulation. Energy deposited by beta electrons along the track in 280 μm thick detector followed Landau fluctuations. Electric charge created in the form of free electrons and holes was divided into buckets, each corresponding to 1 μm of track. The current signal $i_k(t)$ induced on the readout strip k by each individual bucket of charge q moving in electric field of the microstrip detector was calculated according to Ramo's theorem as [10,11]:

$$i_k(t) = q\vec{E}_{wk}\vec{v}(t) + q \sum_{i \neq k} N_{ki}\vec{E}_{wi}\vec{v}(t) \quad (1)$$

\vec{E}_{wi} is the weighting electric field, $\vec{v}(t)$ is the drift velocity of the charge and N_{ki} is the voltage response at the strip i to the unit pulse applied at the strip k .

Readout strips are connected to an amplifier having a low input impedance and they may be assumed to have a well defined potential. Therefore N_{ki} is different from 0 only for interpolation strips i connected to the defined potential via a high (several $M\Omega$) resistance. According to the reciprocity theorem [12] N_{ki} is equal to the fraction of charge induced on strip k if charge q is placed on the interpolation strip. This fraction was calculated with an electrostatic model using the thin wire approximation [13,14]. Results for detectors with every second strip connected to a fixed potential are listed in Table. 1 for different strip pitches and widths. $56 \mu\text{m}$ and $80 \mu\text{m}$ pitches are corresponding to the design of ATLAS analogue and binary module, while $25 \mu\text{m}$ pitch was chosen in order to compare the results of simulation with measurements [15].

If the simulated detector has readout strips only, $N_{ki} = 0$ and the second term in Eq. 1 vanishes.

| strip pitch | strip width | $N_{k,k\pm 1}$ | $N_{k,k\pm 3}$ |
|------------------|------------------|----------------|----------------|
| $25 \mu\text{m}$ | $10 \mu\text{m}$ | 0.351 | 0.063 |
| $56 \mu\text{m}$ | $18 \mu\text{m}$ | 0.329 | 0.060 |
| $80 \mu\text{m}$ | $18 \mu\text{m}$ | 0.300 | 0.057 |

Table 1

Calculated fraction of charge induced on strip k if charge q is placed on the interpolation strip i . Every second strip is connected to readout electronics

The weighting electric field $\vec{E}_{wi} = -\vec{\nabla}V_w$ was calculated by solving Laplace equation $\nabla^2 V_w = 0$ for potential $V_w = 1$ at readout strip i , $V_w = 0$ at all other strips and at the backplane. $\partial V_w(x, y)/\partial y = 0$ was assumed at the surface between strips. Here x is the coordinate perpendicular to the strips in the surface plane and y the coordinate perpendicular to the detector surface. The boundary condition at the x edges was $\partial V_w(x, y)/\partial x = 0$. The equation was solved on a two dimensional discrete uniform mesh of size $\Delta x = 1 \mu\text{m} \times \Delta y = 1 \mu\text{m}$. The weighting potential $V_w(x, y)$ was calculated for a group of 5 strips with the middle strip being the one for which the Ramo field had been calculated.

The electric field in the detector was calculated by solving numerically the Poisson equation for the space charge region in the abrupt junction approximation. Only voltages higher than FDV were considered in the calculations. The boundary conditions at the surface of the microstrip detector were $V = 0$ at all strips, $V = V_{bp}$ at the backplane and $\partial V(x, y)/\partial y = 0$ at the surface in the inter-strip region. Same mesh and boundary conditions at the x edges (\pm half strip pitch) as in calculations of \vec{E}_w were used. The effective space charge

density $e_0 N_{eff}$ used in the Poisson equation was determined from measurements of FDV as:

$$N_{eff} = \frac{2 \cdot \varepsilon_0 \varepsilon_{Si} \text{FDV}}{e_0 W^2} \quad (2)$$

with W the detector thickness and ε_{Si} the dielectric constant of silicon. FDV was determined with the $C - V$ method at room temperature and 1 kHz frequency. The effect of a thin positive space-charge layer at the strip side, (“double junction”) was investigated for irradiated detectors with its parameters taken from [17–19]. Its influence on charge collection efficiency was negligible at any operating point above FDV.

Drift velocity was calculated from $\vec{v} = \mu \vec{E}$, where μ is the mobility of charge q in electric field \vec{E} . Parametrisation of mobility for electrons and holes as a function of temperature, electric field and effective doping concentration was taken from [16]. Diffusion was included in the simulation just in a few test runs. Its effect on charge collection efficiency was found to be negligible and was therefore not taken into account in results presented in this paper.

Trapping times of electrons τ_e and holes τ_h diminished the size of a particular bucket like $\exp(-t/\tau)$. Their values taken from [21] as well as effective doping concentrations determined from the FDV measurements are listed in Table 2.

| Φ_{eq} /cm ² | not irradiated | low fluence 5×10^{13} | high fluence 15×10^{13} |
|---------------------------------|---------------------------|--------------------------------------|-------------------------------------|
| FDV(1kHz) | 60V | 50V | 240V |
| N_{eff} | 10^{12} cm^{-3} | $0.8 \times 10^{12} \text{ cm}^{-3}$ | $4 \times 10^{12} \text{ cm}^{-3}$ |
| $\tau_e(T = 300\text{K})$ | > 500 ns | 27 ns | 9.5 ns |
| $\tau_h(T = 300\text{K})$ | > 500 ns | 66 ns | 24 ns |

Table 2

Parameters used in simulation: FDV, electron trapping time τ_e , hole trapping time τ_h . Φ_{eq} is 1 MeV neutron NIEL equivalent fluence. Irradiated detectors were annealed to the minimum in FDV.

2.2 Shaping electronics

The electronic circuit was composed of a preamplifier followed by a pulse shaping circuit ($CR - RC$ and $CR - RC^2$, respectively). The preamplifier was

considered as an integrator with a response to induced current as:

$$U_{out}(t) = \frac{1}{C} e^{-\frac{t}{\tau}} \int_{-\infty}^t i(t') e^{\frac{t'}{\tau}} dt' \quad , \quad (3)$$

where $i(t')$ is the induced current from Eq. 1, and τ is the product of the integration capacitance ($C = 1$ pF) and the feedback resistor ($R = 1$ M Ω) in the preamplifier circuit.

The differentiation of the signal (CR circuit) was calculated as:

$$U_{out}(t) = U_{in}(t) - \frac{1}{\tau} e^{-\frac{t}{\tau}} \int_{-\infty}^t U_{in}(t') e^{\frac{t'}{\tau}} dt' \quad (4)$$

with $\tau = RC$ the shaping constant and $U_{in}(t')$ from Eq. 3. RC integration in the shaping circuit was calculated by:

$$U_{out}(t) = \frac{1}{\tau} e^{-\frac{t}{\tau}} \int_{-\infty}^t U_{in}(t') e^{\frac{t'}{\tau}} dt' \quad , \quad (5)$$

In the case of $CR - RC^2$ shaping a value of $RC=12.5$ ns resulted in 25 ns peaking time, while in the case of $CR - RC$ circuit values of $RC=50$ ns and 75 ns resulted in peaking time values equal to RC .

3 Charge collection efficiency

The charge collection efficiency (CCE) was defined as the ratio of the most probable cluster height obtained when simulating the detector response to the beta source signal and the height of signal obtained by injecting an instant charge pulse $i(t) = A \cdot \delta(0)$ corresponding to the most probable energy loss of electrons from a ^{90}Sr source. The most probable energy loss was determined by simulation to be equivalent to creation of 23300 electron-hole pairs in the detector volume [20]. Cluster signals were calculated for every track as a sum of signals on strips satisfying the following criteria: at least one (central) strip should have $S/N > 4$ (S/N - signal to noise ratio), all neighbouring strips with $S/N > 2$ are included in a cluster and the sum of S/N over a cluster should be at least 5. Due to cuts used, the cluster signals may depend on noise, particularly for low S/N . It was not the purpose of this study to investigate details of noise influence on measured CCE. Equal noise was assumed for all

three different simulated readout electronics. The noise used as the input for simulation was taken from the measurement [15]. Its value was $ENC = 900 e_0$ for non-irradiated detector and $1000 e_0$ for irradiated detectors.

The most probable cluster height was obtained by fitting a convolution of Landau and Gaussian functions to the histogrammed cluster signals.

3.1 Charge collection efficiency dependence on voltage

Simulated CCE as a function of bias voltage applied to the detector with $25 \mu\text{m}$ strip pitch is shown in Fig. 1.

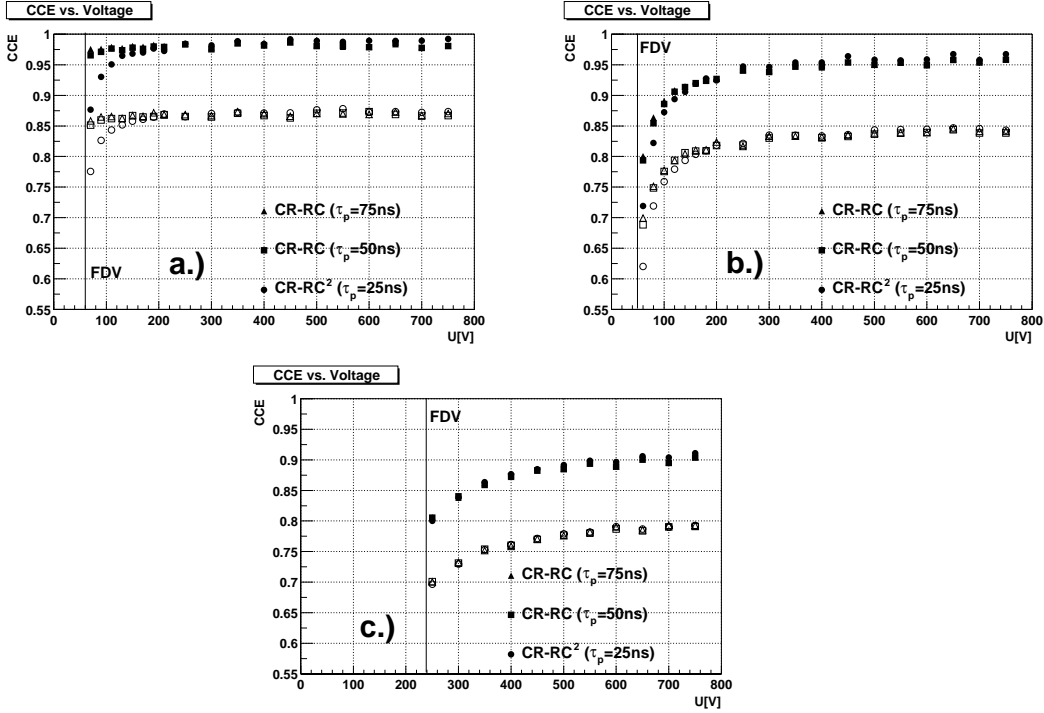


Fig. 1. Calculated CCE as a function of bias voltage at $T=262 \text{ K}$ for a) non-irradiated detector, b) detector irradiated to $\Phi_{eq} = 5 \times 10^{13} \text{ cm}^{-2}$ and c) detector irradiated to $\Phi_{eq} = 15 \times 10^{13} \text{ cm}^{-2}$. Open markers denote CCE if every second strip is being read out. Strip pitch is $25 \mu\text{m}$. Note the suppressed zero on the CCE scale.

Since trapping times before irradiation are long compared to the shaping times, the CCE voltage dependence (Fig. 1a) can be explained by the increase of drift velocity at higher bias voltages, the effect being far more significant at short shaping time. About 150 V above FDV is needed to reach the saturated value of CCE with 25 ns shaping time, while nearly no over-depletion is needed for longer shaping times ($\tau \geq 50 \text{ ns}$). Trapping of the charge in traps created by irradiation becomes the dominant process reducing the CCE above

FDV after irradiation. Since detrapping is long compared to all electronic integration times used, charge once trapped does not contribute to the signal. Therefore after irradiation the difference between different electronic schemes can be hardly observed in Fig. 1b and definitely vanishes at 1c. The effect of trapping can be clearly seen slightly above FDV where a substantial part of charge is trapped due to slow drift. At higher voltages the signal increases further due to faster drift and reduced trapping. There is no clear saturation of CCE even at voltages a few hundred volts above FDV explained by the fact that velocity saturation has not yet been reached along the whole drift path. Since trapping is proportional to the fluence, this effect is more pronounced at the higher fluence.

If every second strip is read out, the most probable signal is reduced (open markers in Fig. 1) as expected from values of $N_{k,i}$ in Table 1.

3.2 CCE of different detectors

Results for CCE with different detector pitches and fixed (25 ns CR-RC²) shaping time are shown in Fig. 2. A few percent lower CCE of large pitch detectors is due to smaller coupling to neighbouring strips (see Table 1).

3.3 Temperature dependence of CCE

Temperature dependence of CCE was also studied by simulation. Trapping time was scaled as $\tau \propto \frac{1}{\sqrt{T}}$ due to the change in thermal velocity. Another effect of temperature is the change of mobility ($\mu \propto T^{-2.0}$ and $T^{-2.18}$ for electrons and holes, respectively). Lower temperature increases drift velocity and trapping time, thus increasing CCE. This can be clearly seen in Fig. 3. The effect is more pronounced at lower voltages and higher fluences where trapping plays an important role in CCE.

3.4 Influence of timing

Due to high collision rate at LHC experiments, signals from the front end will be sampled and stored into a pipeline until the trigger decision. In order to get maximum signal the output from the preamplifier should be sampled at peak with an adequate delay with regard to the bunch crossing. This delay depends on the distance of the detector from the collision point and the shape of the induced current. While the detector position is fixed, the induced current shape changes with applied voltage. A proper delay maximizing CCE

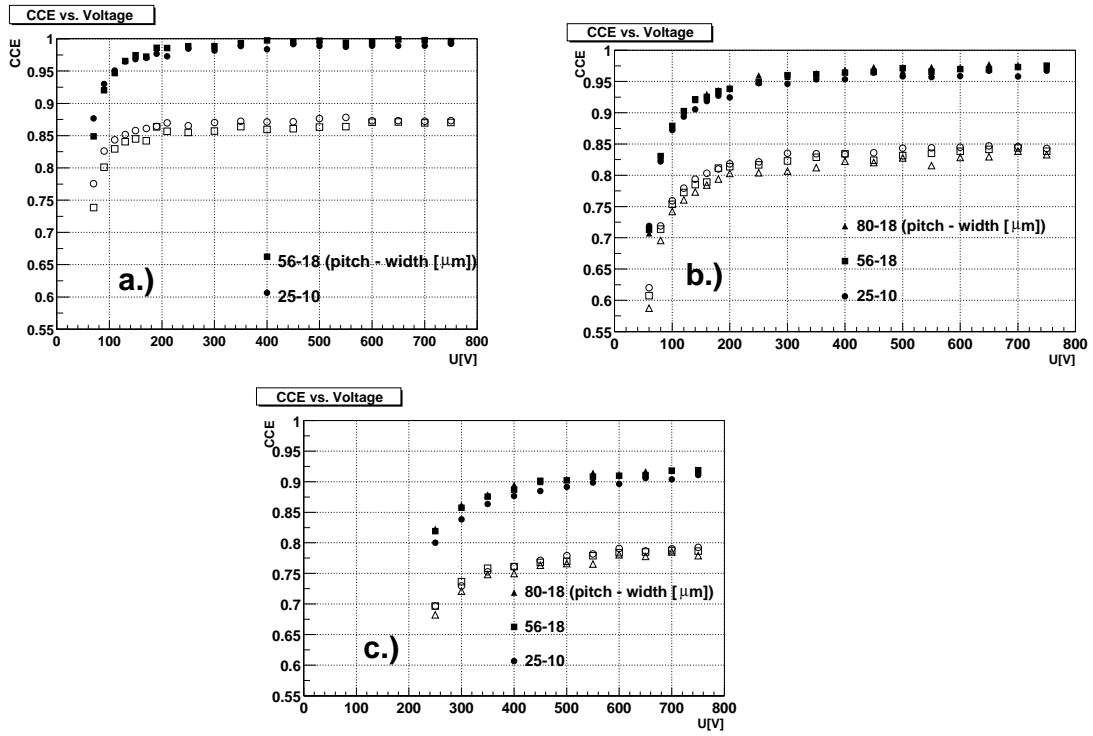


Fig. 2. Calculated CCE of detectors with different pitches as a function of applied voltage. Fast 25 ns ($CR-RC^2$) shaping was used at $T = 262$ K. a) non-irradiated, b) irradiated to low fluence, c) irradiated to high fluence. Open markers denote detectors with every second strip read-out.

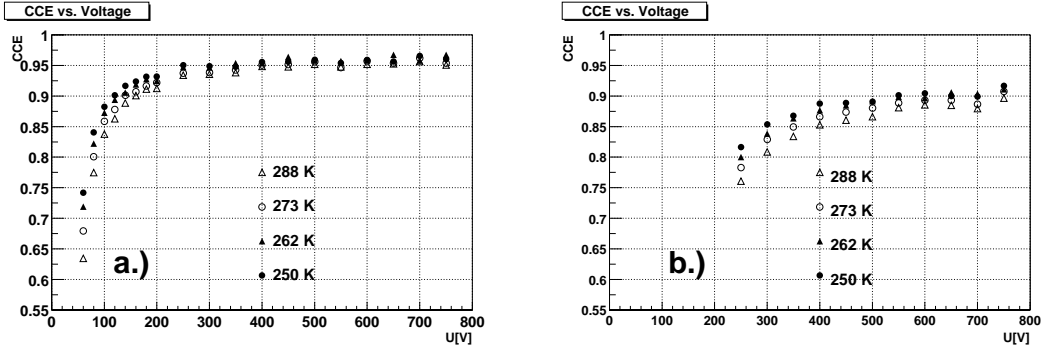


Fig. 3. Temperature dependence of CCE with 25ns $CR-RC^2$ shaping at a) low fluence; b) high fluence

should be chosen for each detector module. We have determined the CCE for various delays in the range between 25 ns and 40 ns and different bias voltages on detector (Fig. 4). Detector with 50 μm readout pitch having one interpolating strip has been used in this simulation. For a comparison measured values with such a detector and a fixed delay [15] having a value of 25 ns are also plotted. Voltage dependence of measured CCE is in good agreement with simulated values. Somewhat larger discrepancy at higher fluence and bias voltages slightly above FDV could be explained by an uncertainty in

the measured value of FDV which is used as input for simulation. Simulated values obtained with optimal timing (sampling in the peak of signal, the delay being voltage dependent) are also plotted. A proper fixed delay (25 ns) gives values close to the optimal if voltage applied on the detector is sufficiently higher than FDV.

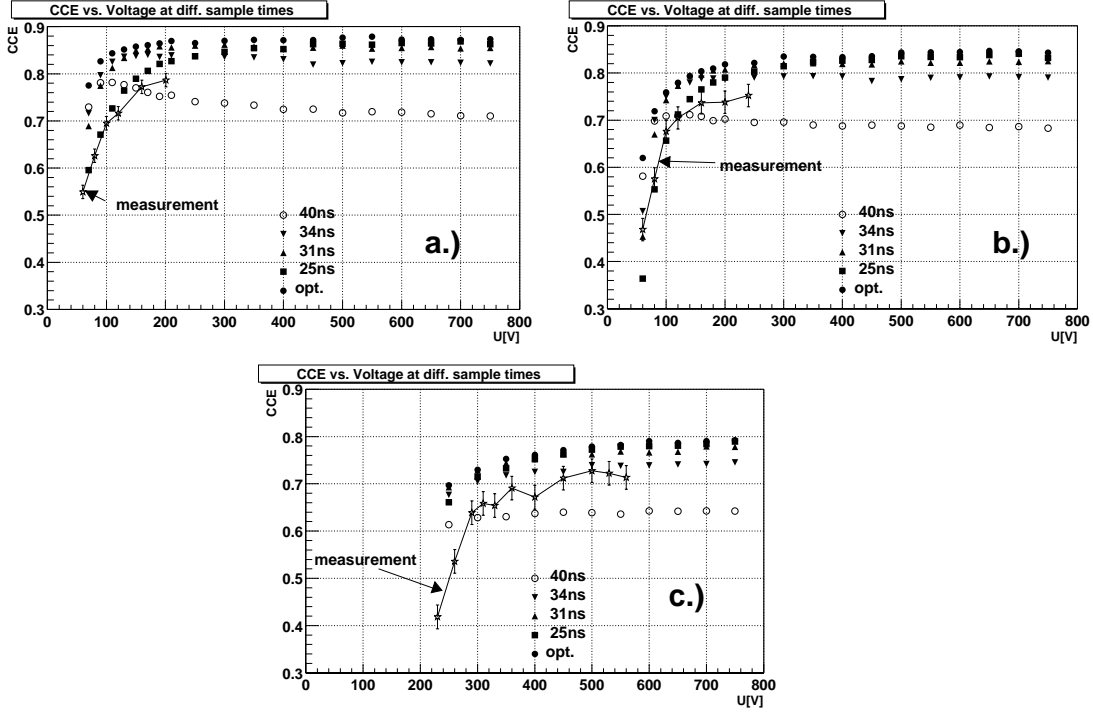


Fig. 4. Simulated CCE with different delays of signal sampling compared to measurements with a fixed 25 ns delay for a) non-irradiated detector, b) irradiated to low fluence, c) irradiated to high fluence. The measurement and simulation were performed with 25 ns CR-RC² shaping.

The optimal delay and the corresponding CCE as a function of applied voltage are shown in Fig. 5. As expected the best sampling time approaches the nominal peaking time as the voltage increases. On the other hand the CCE increases with voltages well beyond the depletion voltage. The slope of this rise is around $0.9e_0/V$ for detector irradiated to low fluence and $2.2 e_0/V$ for detector irradiated to high fluence.

4 Conclusions

Simulation has shown that bias voltages beyond full depletion voltage are needed for high CCE even for non irradiated silicon microstrip detectors if read out with 25 ns shaping electronics is used. In this case, about 150 V of over-depletion is needed for non irradiated detector to reach CCE $\sim 98\%$. For irradiated detectors charge trapping is dominating the loss of signal and

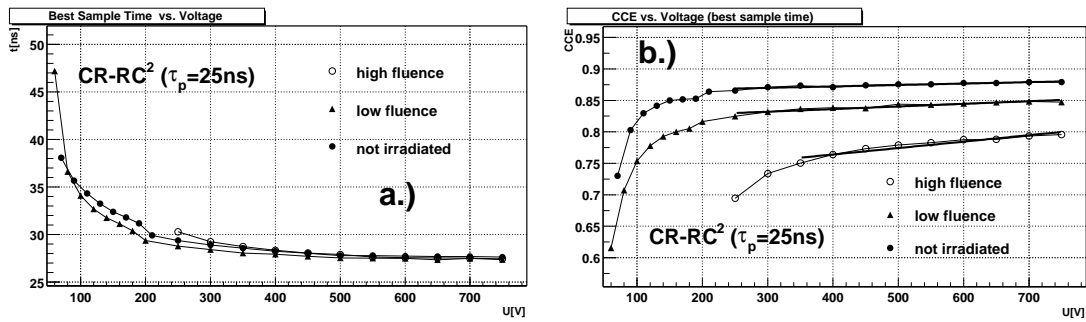


Fig. 5. a) The optimal delay for detector with $50\ \mu\text{m}$ read-out pitch and one interpolation strip with 25 ns CR-RC² shaping circuit; b) CCE efficiency for optimal delay of sampling. Electron hits detector at $t=0$.

CCE becomes nearly independent on shaping times. Again at least 150 V of over-depletion is needed to obtain high CCE. Signal does not saturate even at voltages a few hundred volts above the FDV.

References

- [1] ATLAS TDR 5, CERN/LHCC/97 17
- [2] F. Lemeilleur et al., Nucl. Instr. and Meth. A 360 (1995) 438.
- [3] M. Moll et al., Nucl. Instr. and Meth. A 426 (1999) 87.
- [4] E. Fretwurst et al., Nuclear Instr. and Meth. A388 (1997) 356.
- [5] Bacchetta et al., Nuclear Instr. and Meth. A 426 (1999) 16.
- [6] L. Andricek et al., Nuclear Instr. and Meth. A 409 (1998) 184.
- [7] C. Leroy et al., Nuclear Instr. and Meth. A 388 (1997) 296.
- [8] W. Dabrowski et al., Nuclear Instr. and Meth. A 356 (1995) 241.
- [9] J. Leslie et al., IEEE 40, (1993) 557
- [10] S. Ramo, Proc. IRE 27 (1939) 584.
- [11] E. Gatti et al., Nucl. Instr and Meth. 193 (1982) 651.
- [12] V. Radeka, Ann. Rev. Nucl. Part. Sci. 38 (1988) 217.
- [13] P. Chochula et al.: Nucl. Instr. and Meth. A377 (1996) 409.
- [14] U. Kötz et al.: Nucl. Instr. Meth. A235 (1985) 481.
- [15] V. Cindro et al., Nucl. Instr. and Meth. A439 (2000) 337.
- [16] S. Selberherr, W. Hansch, M. Seavey, and J. Slotboom., *The Evolution of the MINIMOS Mobility Model. Solid-State Electron.*, 33(11):1425–1436, 1990.

- [17] Z. Li and H. Kraner, *Journal of Electronic Material* 21 (1992) 701.
- [18] L. J. Beattie et. al., *Nuclear Instr. and Meth. A* 418 (1998) 314.
- [19] D. Passeri et al., *Charge Collection Analysis of Low-Resistivity Si-Microstrip Detectors* , 4th Rose Workshop on Radiation Hardening of Silicon Detectors, CERN/LEB 98-11 533.
- [20] G. Kramberger, Diploma thesis, University of Ljubljana, 1995
- [21] H.W. Kraner et al., *Nuclear Instr. and Meth. A*326 (1993) 350.
- [22] F. Anghinolfi et al., *IEEE Trans. Nucl. Sci.* NS-44 (1997) 298.
- [23] Gadomski et. al, *Nuclear Instr. and Meth. A*320 (1992) 217.